https://doi.org/10.5194/egusphere-2026-3292
Preprint. Discussion started: 26 June 2026

Probing the Koillismaa Deep Intrusion in Northern Finland using Advanced Seismic Imaging

Brij Singh[1], Andrzej Górszczyk[1], Michal Malinowski[1,2], Tuomo Karinen[2]

[1]Institute of Geophysics, Polish Academy of Sciences Warsaw, Księcia Janusza 64, 01-452 Warsaw, Poland
[2]Geological Survey of Finland, Vuorimiehentie 5, 02151 Espoo, Finland

Correspondence to: Brij Singh (bsingh@igf.edu.pl)

Abstract.

The Koillismaa–Näränkävaara Layered Igneous Complex (KLIC) has been the subject of continuous studies due to its potential to host several critical raw materials, mostly of the Ni-Cu-PGE sulphide type. The KLIC is characterised by a ~50–60 km-long geophysical anomaly in which the magnetic high is followed by a shifted gravity high response, believed to be caused by the Koillismaa Deep Intrusion (KDI), but the exact origins remain unknown. A regional reflection seismic profile was acquired under the SEEMS DEEP project (2022–2025) to define the spatial geometrical architecture of the KDI. Initial processing using standard time-domain and conventional depth imaging revealed its first-order large-scale structure, indicating a funnel-shaped geometry and confirming it as a geologically complex target. In this study, we apply advanced seismic imaging methods, better suited to complex geologies, to further improve the imaging of the KDI. Ray-based (least-squares)Kirchhoff prestack depth migration and wave-equation-based reverse time migration (RTM) were used for this purpose. A high-resolution P-wave velocity model was built using acoustic full waveform inversion (FWI), while first arrival traveltime tomography was applied to build the starting model for FWI. Wave-equation-based, joint RTM-FWI workflow provided the optimum imaging of the KDI setting. A comprehensive reinterpretation of the KDI was done using the multi-method approach integrating gravity, magnetic and electromagnetic surveys. The available borehole information and common earth model for the study area were used as constraints. Shallow seismic reflectivity correlated well with the mafic dykes observed in the magnetic data. The exact origin of these dykes was earlier unknown and was attributed to the observed magnetic high in the KLIC area. Advanced seismic imaging revealed a previously unrecognized, more laterally extensive top of the KDI whose full extent was previously unknown. It is also interpreted that the denser mafic intrusion (KDI) defined by this extensive top may have increased the net vertical mass distribution in the area, because of which a shifted gravity response with respect to the magnetic high has been observed. A new hypothesis on the angular ascent of the magma towards the surface is also proposed based on the mapped seismic reflectivity associated with the mafic intrusion.

Keywords

Land seismic; Mineral Exploration; FWI; Least-squares Migration; RTM

https://doi.org/10.5194/egusphere-2026-3292
Preprint. Discussion started: 26 June 2026

1. Introduction

Mineral resources are foundational to the global economy. They are shaping modern society by driving industrial growth, supporting infrastructure development, and playing a crucial role in achieving sustainable energy goals (Montana et al., 2025). With the demand for raw materials at an all-time high, the 2.44 Ga KLIC in northern Finland holds great possibilities to host several orthomagmatic occurrences, for example, Ni-Cu-Co-PGE and Cr-V-Ti-Fe type deposits (Hayward, 2024; Simandl and Paradis, 2022). These deposits, for example, are essential for producing electric vehicle batteries, speciality steel, clean energy technologies and defence applications such as high-strength aerospace alloys. The KLIC comprises of two surface-exposed intrusions, Koillismaa in the west and Näränkävaara in the east. They are linked by the gravity and magnetic high anomaly caused by the deep-seated KDI (Karinen, 2010; Salmirinne and Iljina, 2003). Over the past decades, several geological, geochemical and geophysical studies have been conducted to establish the compositional and structural architecture of the KDI. Salmirinne and Iljina (2003) interpreted its shape to be tubular/funnel-shaped with a width of ~2.5-4 km based on the observed Bouguer anomaly. In 2018 and 2022, the Geological Survey of Finland (GTK) conducted 2D surface seismic and vertical seismic profiling (VSP) surveys in the central part of the KDI to map its seismic reflectivity, and to investigate its geometrical structure (KOSE2018 survey; Gislason et al., 2019; Malinowski et al., 2023; Tirroniemi et al., 2024). In 2020, GTK made a drilling (Koillismaa borehole) adjacent to the KOSE survey and confirmed the presence of the mafic-ultramafic rocks at a depth of ~1.4 km from the surface, coeval with the exposed intrusions of the KLIC (Karinen et al., 2021).

In 2022, ERA-MIN3 sponsored the SEEMS DEEP project, which aimed to further understand the geometrical architecture of the KDI by acquiring comprehensive seismic (both 2D and 3D), controlled-source electromagnetics (CSEM), magnetotellurics (MT), induced polarisation, and electrical resistivity tomography datasets (Autio et al., 2024). Standard time-domain and conventional seismic depth imaging successfully mapped the large-scale architecture of the magma conduit (KDI) and established it as a geologically complex target. Several near-surface and regional reflective packages were interpreted as diabase dykes, overthrust faults and major lithological contacts in the area (Singh et al., 2025). A funnel-shaped geometry of the KDI was established with a laterally extensive top as predicted by Salmirinne and Iljina (2003). A Common Earth Model (CEM) was prepared based on the seismic surveys and potential field data with constraints from Koillismaa borehole data (Malinowski et al., 2025; Salmirinne and Iljina, 2003). This study further improves the seismic imaging of the KDI using cutting-edge techniques such as FWI, least-squares Kirchhoff prestack depth migration (LS-KPreSDM), and RTM using the regional 2D seismic profile (Burschil et al., 2025; Norman et al., 2024; Schijns et al., 2023; Ziramov et al., 2023). A joint wave-equation-based RTM-FWI workflow, which is rarely applied for mineral exploration purposes, was applied to image the geologically complex and structurally intricate KDI (Singh et al., 2022).

A 3D acoustic-FWI was used to build a high-resolution P-wave velocity model (Ravaut et al., 2004; Malinowski et al., 2011; Baeten et al., 2013; Afanasiev et al., 2014; Adamczyk et al., 2015; Stopin et al., 2014). First arrival traveltime tomography

https://doi.org/10.5194/egusphere-2026-3292
Preprint. Discussion started: 26 June 2026

(FATT) was applied to build the starting model for FWI (Bräunig et al., 2020; Hloušek et al., 2025; Singh et al., 2019). Data preprocessing and inversion strategy were developed for the FWI, curated for the KLIC dataset. Velocity models derived from both approaches, i.e. FATT and FWI, were used for seismic depth-domain imaging, e.g., KPreSDM, LS-KPreSDM and RTM (Ding and Malehmir, 2021; Singh et al., 2019,2022). The joint RTM-FWI workflow provided the optimal seismic imaging in the area. An integrated geophysical reinterpretation of the study area was undertaken using available magnetics and gravity data, together with joint CSEM-MT inversion results obtained within the SEEMS DEEP project (Vedrine et al., 2024). The interpretation was constrained by borehole data, providing direct subsurface information and guided by the common earth model (CEM). This multi-method framework aligns with, and fulfils one of the key objectives of the SEEMS DEEP project.

New seismic imaging revealed that the previously interpreted top of the KDI extends farther north. This lateral extension is inferred to have shifted the net vertical mass distribution in the KLIC area, leading to a spatial offset shift between the gravity high and the magnetic high responses. This interpretation is supported by a strong correlation between seismic reflectivity and a corresponding high-resistivity zone delineated in the joint CSEM-MT result. At shallower depth, the seismic reflectivity showed good agreement with mafic dykes mapped from aeromagnetic data, whose origins were previously remained uncertain. Based on the high-fidelity reflectivity associated with the KDI, we also propose a new hypothesis to explain the shift between the gravity and magnetic anomalies in the KLIC area. The hypothesis suggests that the gravity high may have been attributed from an oblique ascent of magma towards the surface, rather than the purely vertical emplacement previously assumed.

This article is organized as follows. First, a brief introduction to the KLIC area is provided, including its geology, the petrophysical analysis of the Koillismaa borehole, and the CEM building. The “Materials and Methods” section then discusses seismic data acquisition and processing, along with a brief introduction to FWI. The following section presents the results obtained from the 2D seismic data. First, the velocity model building (VMB) workflow is described, including FATT, data preprocessing, the inversion strategy for FWI, and the FWI results. The second part presents the results obtained from KPreSDM, LS-KPreSDM, and RTM. Finally, the interpretation and discussion section examines the obtained results and compare them with the available CEM, joint CSEM-MT, gravity, and aeromagnetic data. The article concludes with a summary of the study.

2. Koillismaa-Näränkävaara Layered Igneous Complex

2.1 Geological setting of the area

The Tornio–Näränkävaara Belt (TNB; Alapieti and Lahtinen, 2002) extends from the Finnish–Swedish border to the Finnish–Russian border located along the contact zone between the basement and the overlying Palaeoproterozoic greenstone and schist belts, and represents a ~2.44 Ga magmatic system in northern Finland. These intrusions are considered of high economic interest with a continuous history of mineral exploration and mining since the early 20th century. TNB is part of the larger

https://doi.org/10.5194/egusphere-2026-3292
Preprint. Discussion started: 26 June 2026

Fennoscandian Schield, which hosts numerous ~2.51–2.43 Ga mafic-ultramafic layered intrusions which were formed during the magmatism associated with an extensional phase that led to the breakup of Archaean cratons (Köykkä et al., 2022; Skyttä et al., 2019). The KLIC forms the easternmost part of TNB, and is composed of two surface exposed intrusions, the Koillismaa Intrusion and the Näränkävaara Intrusion (Fig. 1). The Koillismaa intrusion was emplaced into the boundary between the Archaean basement and the overlying supracrustal sequence that now forms the lowermost stratigraphic parts of the Kuusamo Schist Belt (top-left corner, Fig. 1; Köykkä et al., 2022). The intrusion is composed of mafic-ultramafic cumulates and was later tectonically dismembered into distinct blocks, which are now mostly oriented in an E–W direction (Karinen, 2010). The Näränkävaara intrusion is surrounded by the Archean gneiss and has largely retained its original position. The intrusion is mostly composed of ultramafic cumulates (Järvinen et al., 2020).

The study area (black rectangle, Fig. 1) is located in the central part of the KDI, where the surface geology is dominated by homogeneous orthogneisses of the Archaean basement, although a narrow belt of banded iron formations (BIFs) and irregular bodies of greenstone occur in the southern part (Makkonen, 1972). These lithologies may be related to the Archaean greenstone belt known east of the study area (Järvinen et al., 2023). Multiple diabase dykes are also present, likely intruded along fractures and faults. At depth, the unexposed KDI is composed of mafic–ultramafic rocks, including peridotites, pyroxenites, and gabbronorites (see Fig. 2f).

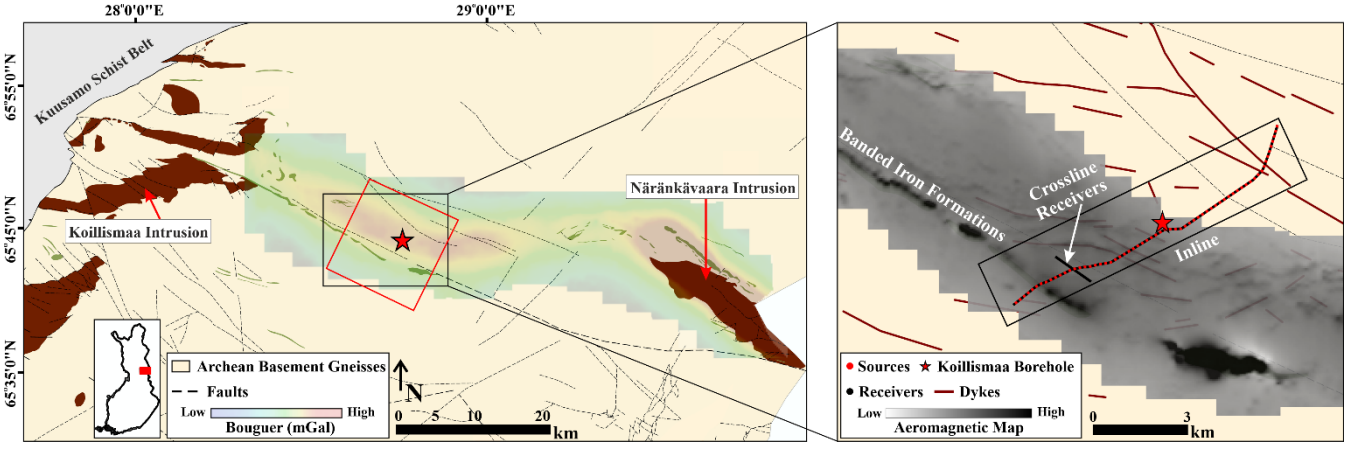

Figure 1. Generalized geological map of the KLIC (from "Bedrock of Finland v2.3 at the scale 1:200 000"). The study area location is shown on the map of Finland in the bottom-left inset. Red rectangle marks the extent of the CEM model (section 2.3). A black rectangle marks the study area for which a zoomed section is shown. Red points overlapping the black points mark the source and receiver positions overlaid on the total magnetic intensity shading (grey surface; white (low) & black (high)). The black rectangle in the zoomed section shows the computational domain for the 3D velocity model building and depth imaging.

https://doi.org/10.5194/egusphere-2026-3292
Preprint. Discussion started: 26 June 2026

2.2 Petrophysical study

Petrophysical and laboratory studies were conducted on the drill core samples collected at ~1 m intervals (18 – 1594 m (1227 samples)), enabling the classification of different lithologies and rock types (red star in Fig. 1; Heinonen et al., 2022; Nousiainen et al., 2022). Geochronological study performed on the collected mafic–ultramafic lithologies confirmed that the magma conduit is coeval with the ~2.44 Ga Koillismaa and Näränkävaara intrusions (Karinen et al., 2025). Figure 2 shows P-wave velocity, density, acoustic impedance, reflection series, synthetic seismogram and a simplified lithology of the Koillismaa borehole. The reflection series is based on the laboratory measurements on the core samples, and the synthetic seismogram is produced using the Ormsby wavelet (20-30-90-110 Hz). The synthetic seismogram shows a strong reflection from the mafic-ultramafic rocks & dykes with respect to the overlying granite and the Archean gneissic complex. The surface bedrock lithology is mainly composed of homogenous orthogneisses and cross-cutting diabase dykes.

2.3 Common Earth Model

The CEM of the KDI area was made available (model limit is shown by a red rectangle in Fig. 1). Given the limited geological constraint to just one borehole and a few surface outcrops, the main component of the CEM was the 2D and 3D seismic imaging obtained under the SEEMS DEEP project. Susceptibility modelling and the existing potential field inversion results were also used with constraints from the borehole data (Salmirinne and Iljina, 2003). The CEM covers an area of approximately 13 x 13 km (Fig. 3). The CEM was mainly classified into the following lithologies: Archean gneissic basement, banded iron formations (BIFs), greenstones, granite and mafic-ultramafic intrusion. A few faults were also mapped based on the seismic study. CEM is shown without the Archean basement and granite for better visibility. Also, the mafic and ultramafic part of the intrusion is combined for better clarity. For full details, please refer to Malinowski et al., 2025.

3. Materials and Methods

3.1 Seismic Data Acquisition and Processing

A regional seismic profile was previously acquired under the SEEMS DEEP project with an approximate length of 10.5 km (oriented NE-SW). A 22-tonne Mark IV Vibroseis truck (48000 lbs peak force) was used as the source, generating 20 s sweeps from 20-160 Hz (+1 dB gain), repeated 3 times at each location. Geospace's GS-ONE, three-component land geophones with a natural frequency of 5 Hz were used as the receiver. A uniform receiver spacing of 15 m and an overlapping shot spacing of 30 m were used. The acquired data were of good quality with clear first breaks visible for ~4-5 km of offset distance for the majority of the shots, except for the shots in the western end for which first breaks were clearly visible for the full offset range.

https://doi.org/10.5194/egusphere-2026-3292
Preprint. Discussion started: 26 June 2026

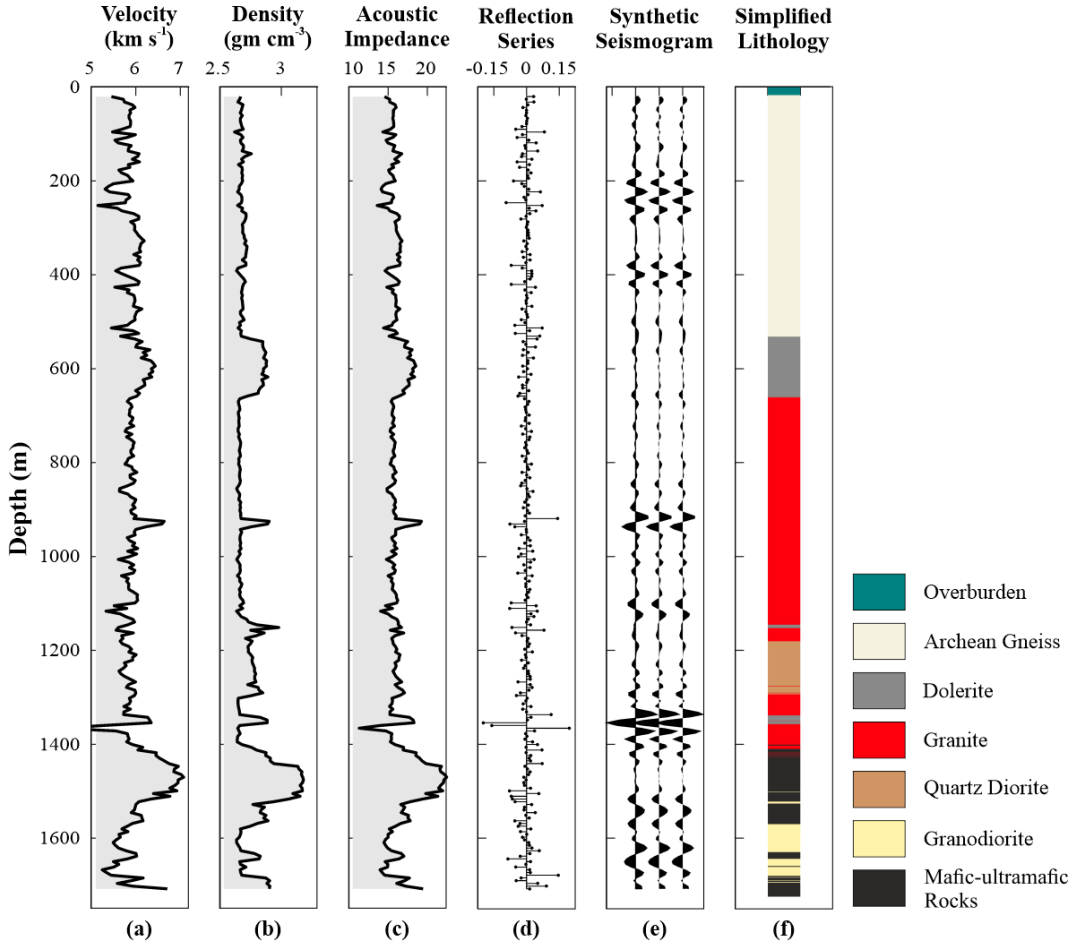

Figure 2. Koillismaa borehole laboratory petrophysics (red star, Fig. 1). (a) P-wave velocity, (b) density, (c) acoustic impedance, (d) reflection series, (e) synthetic seismogram, and (f) shows the simplified lithology. The synthetic seismogram shows a strong reflection from the mafic-ultramafic rocks to the overlying granite & the Archean gneissic complex.

In this study, we used the same processed data presented by Singh et al. (2025) for seismic imaging; no additional steps were applied. Previous data processing followed the standard workflow used for the hardrock setting. First, vertical component of the data was extracted and a rectangular geometry was set up. Bad/noisy traces were removed and a focused emphasis was put on handling the near-surface weathered layer through statics correction. Spherical divergence correction, automatic gain control and a combination of spiking and predictive deconvolution were applied to the dataset. An airwave mute, 1D median filter and bandpass filter were used to remove the ground roll and shear waves. Curvelet denoising was applied to enhance the coherency of the signal (Górszczyk et al., 2015). Normal moveout and dip moveout corrections (DMO) were applied using a constant velocity of 6 km/s. Prestack, post-stack & DMO followed by post-stack time migration, and depth-domain KPreSDM were applied using the constant velocity. Final migrated shot gathers were stacked and analysed during the final interpretation.

https://doi.org/10.5194/egusphere-2026-3292
Preprint. Discussion started: 26 June 2026

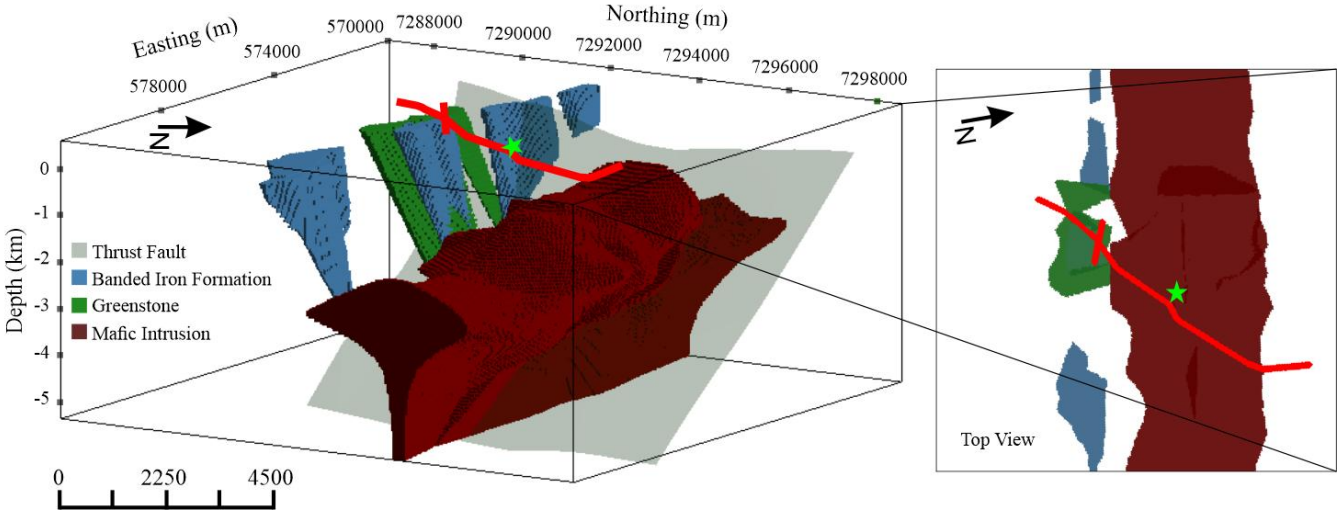

Figure 3. Common Earth Model. The brown body shows the mafic intrusion (KDI), the grey surface shows the regional thrust fault, the blue surface marks the BIFs, and the green surface shows the greenstones. The seismic profile is overlaid on the top of the CEM with receiver points marked in red and the Koillismaa borehole as a green star (same as red star in Fig. 1). The top-view of the CEM is shown on the right panel.

3.2 Full Waveform Inversion

Standard time-domain imaging in the hardrock environment is optimal for simpler geologies, i.e., with gentle dips. KLIC is both geologically and structurally a complex target which requires advanced wave-equation based imaging solutions such as RTM, or least-squares RTM. The biggest challenge in this is the non-availability of a robust high-resolution velocity model which can be derived using FWI. FWI is a least-squares local-optimization method used to build physical parameters of the subsurface by minimizing the difference between the observed and predicted data (Tarantola, 1986; Virieux and Operto, 2009). Limited, but there are now a few successful case studies applying FWI for mineral exploration purposes (Afanasiev et al., 2014; Singh et al., 2022; Schijns et al., 2023). A 3D acoustic-FWI framework in the time domain developed by the SEISCOPE consortium was applied for our study. As FWI is a local-optimization technique, it requires a starting model which must satisfy a cycle-skipping criterion. The FATT-derived velocity model was used for this purpose (section 4.1.1). During FWI, the velocity model was updated iteratively and the gradient of the misfit function was calculated using the graph-space optimal-transport based objective function (Métivier et al., 2018). A Gaussian smoothing operator defined by the correlation length in x, y, z-direction and local wavelength is applied to regularise the gradient after each FWI iteration. The steepest-descent optimization scheme was used using the SEISCOPE Optimization Toolbox (Métivier and Brossier, 2016).

https://doi.org/10.5194/egusphere-2026-3292
Preprint. Discussion started: 26 June 2026

4. Application to the Koillismaa 2D Seismic Data

4.1 Velocity Model Building

4.1.1 Starting Model

FWI requires a starting model with an accuracy to predict the waveforms within half the dominant period present in the data. As a standard approach in the oil & gas industry, usually this starting model is based on the reflection tomography. Such an approach is not valid for the seismic data acquired in the hardrock environment; it often lacks coherent reflections. FATT has been successfully applied in several case studies in the hardrock environment and hence was preferred (Bräunig et al., 2020; Hloušek et al., 2025; Singh et al., 2019, 2022). Manual picking of ~205,000 first arrivals (~75%) was done due to the higher noise level in the data, and later quality checked (QC). Geotomo TomoPlus software was used to build the P-wave velocity model, which has the implemented traveltime inversion framework defined by Zhang and Toksoz (1998). A uniform grid spacing of 30 m was used for traveltime calculations in the inline and crossline direction, and 15 m in depth with a grid dimension of 351 x 71 x 68 (inline x crossline x depth). Inversion was performed at a grid spacing of 60 x 60 x 30 m. The computational domain for FATT is shown in Figure 1 (black rectangle in the zoomed section). A final root-mean-squared (RMS) value of ~8 ms was obtained after 10 iterations. The starting depth (top of the velocity model) was kept at 300 m in elevation to accommodate all the sources and receivers well below this elevation level. The same computational domain and the starting elevation were used for FWI and all subsequent depth imaging results (section 4.2) presented in this article.

Figure 4 shows results for the FATT velocity model. Figure 4a shows the generalized geological map with the overlaid seismic profile (in black), and Koillismaa borehole (red star) for the comparison of velocity details with the surface-mapped geological events, such as faults (dashed-black lines), mafic dykes (red lines), and BIFs. Higher velocities in the range of ~2 km/s in the near surface were observed (just below the source and receivers, Fig. 4b). A quick jump in the velocities was attained from ~2 km/s to ~4.5 km/s within the few tens of meters, typical for hardrock settings (compare Figs. 4b and 4c). Figure 4d shows the velocity model at the inline position marked by red lines in Figs. 4b and 4c. A maximum depth penetration of ~0.5 km was observed with a maximum velocity value of ~6 km/s (Fig. 4d). The obtained velocities were consistent with the velocities observed in the laboratory studies (see Fig. 2a). The accuracy of the FATT velocity model was verified by inspecting the predicted times with the manual first arrival picks for various shot gathers along the profile. As the last step, the velocity model was smoothed to remove artefacts produced during the inversion that might have leaked from the acquisition footprint. This was done by splitting the velocity model into two parts: the top part with the strong velocity changes in the first ~150 m (smaller Gaussian smoothing operator) and the bottom part with the smoother velocity variation (larger Gaussian smoothing operator).

https://doi.org/10.5194/egusphere-2026-3292
Preprint. Discussion started: 26 June 2026

4.1.2 FWI: Data preprocessing and Inversion

The main aim of the data preprocessing workflow was to transform the acquired data (recorded within an elastic medium) into the acoustic approximation. Data preprocessing focused on removing elastic effects (surface waves) & attenuation while preserving the first arrivals and improving the SNR & coherency of the signal. Surface-consistent amplitude balancing was applied to average the shots and receiver amplitudes by minimizing the effects of the highly variable near-surface layer as well as the source-receiver coupling. This step was highly effective during the source wavelet estimation at a later stage. Then, a predictive deconvolution was applied to better preserve the first arrivals. This was followed by FX-deconvolution to improve the coherence of the signal. Frequency filtering tests revealed the first arrivals with acceptable SNR not visible below 18-20 Hz. We inverted a single frequency band of the data defined by a bandpass filter (1-10-25-50 Hz). An external mute function was carefully designed to keep the diving waves and to effectively remove the shear and surface waves. Bad/noisy traces were removed during first arrival picking (see Fig. 8). Trace normalization was applied to remove the viscoelastic response, and equal weightage within the misfit function was provided to receivers at all offsets. Finally, the data was transformed into the local coordinate system. The data preprocessing workflow is summarized in Table 3. Figure 5 shows a comparison of raw data and the data after the preprocessing. After preprocessing, the first arrivals are better preserved with improved coherence of the signal.

Inversion was performed keeping a constant density of 2850 kg/m^3. A smoothed version of the FATT velocity model was used as the starting model. Both the forward modelling and inversion were performed on the same grid dimension of 351 x 71 x 68 (inline x crossline x depth) with a uniform grid spacing of 30 m. An effective offset range of ~5 km was available for FWI (see histogram, Fig. 6a). A maximum of 200 ms of preprocessed data was used for inversion (red lines, Fig. 5b). The first step in the inversion workflow was the estimation of the source wavelet. For land acquisitions, wavelet estimation is highly influenced by several factors such as source-receiver coupling, near-surface heterogeneous weathering layer, local velocity conditions, etc. Here, we applied the linearized approach of Pratt (1999). An averaged source wavelet for all shots (Fig. 6b), and an individual source wavelet for each shot were estimated. In both cases, the source wavelets resembled the minimum-phase equivalent of the vibroseis sweep signature. Inversion was tested using both approaches. In the latter case, scaling and handling of the synthetic amplitudes against the observed data were difficult, and several artefacts were introduced in the model. Therefore, the single averaged source wavelet was utilized. Traces within the first kilometre range from the shot position were implicitly muted to restrict the strong elastic effects that could not be perfectly removed during the data preprocessing (see Fig. 8). A graph-space optimal-transport (GSOT) objective function with Wasserstein distance of 20 ms produced the optimum results (Métivier et al., 2018). GSOT considers the global shape of the signal rather than a sample-by-sample approach (L2-norm). This is advantageous in mitigating the cycle-skipping and has more resilience in handling the noisy datasets. The gradient was smoothed after each iteration. FWI was run for 10 iterations until a negligible drop in the cost function was observed.

https://doi.org/10.5194/egusphere-2026-3292
Preprint. Discussion started: 26 June 2026

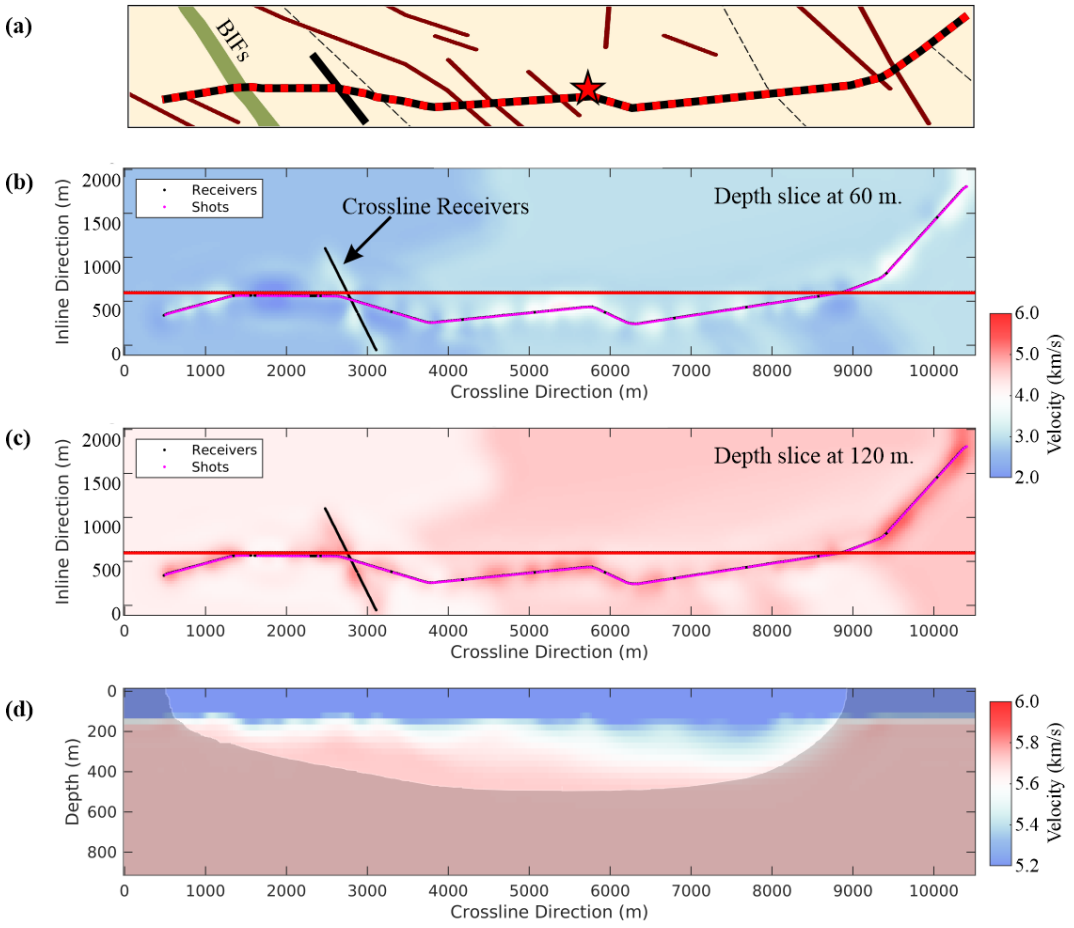

Figure 4. FATT velocity model. (a) Stripe of the geological map restricted to the computation domain (see Fig. 1), (b) and (c) are the depth slices at 60 m and 120 m from the top (300 m a.s.l.), and (d) velocity model restricted by the ray coverage (grey area = no coverage). The red line shows the inline location for which the velocity model is shown in (d). Shots overlapping the receivers are shown as red and black points. Red star marks the borehole location (see Fig. 1).

Table 3. Data preprocessing for FWI

Data Preprocessing
Read Data
Surface-consistent amplitude balancing
Predictive deconvolution
FX-deconvolution
Bandpass filtering [1-10-25-50]
Muting (first arrival based)
Noisy traces removed (first arrival based)

https://doi.org/10.5194/egusphere-2026-3292
Preprint. Discussion started: 26 June 2026

Trace Normalization

Rotation to the local coordinate system

Write data

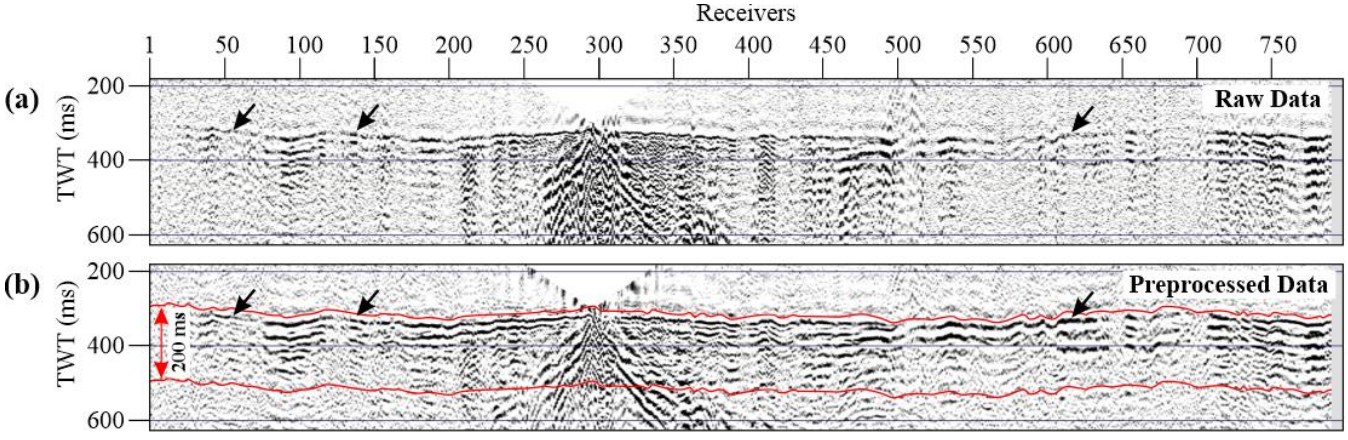

Figure 5. FWI preprocessing. (a) and (b) shows raw and preprocessed data after applying a linear moveout (LMO) with a constant velocity of 5500 m/s and a bulk shift of 100 ms. Red lines mark the range of data comprising the refracted/diving waves used for the FWI without the mute applied. Black arrows mark the areas of significant improvement.

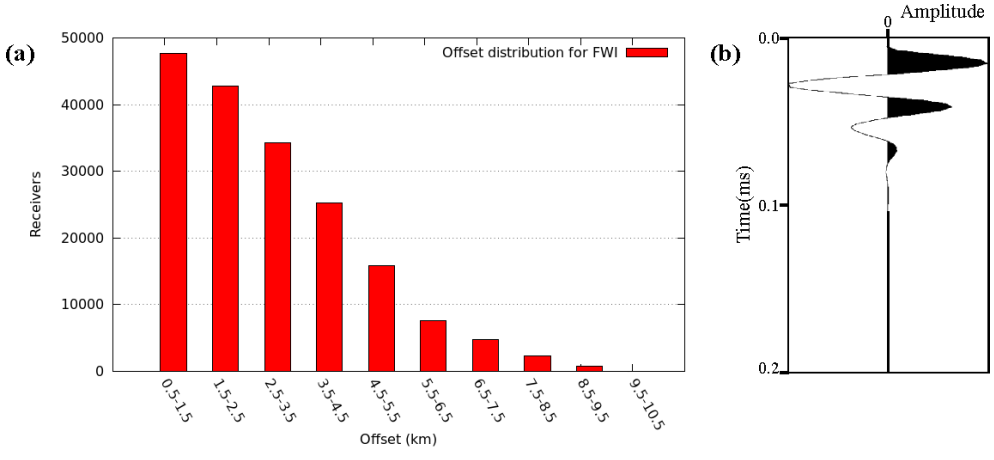

Figure 6. (a) Histogram for offset distribution for FWI, and (b) shows the estimated source wavelet using all shots.

4.1.3 FWI results and QC

Figure 7 shows the result for the FWI velocity model compared to FATT for the same inline location shown in Figure 4d. Figure 7a shows the generalized geological map with the overlaid seismic profile and Koillismaa borehole (same as Fig. 4a). Compared to the FATT velocity model with velocity details limited to the first few hundred meters (Fig. 7b), FWI model is higher in resolution with better depth penetration and structural details (~1 km in depth, Fig. 7c). An accumulation of higher

https://doi.org/10.5194/egusphere-2026-3292
Preprint. Discussion started: 26 June 2026

layered velocities (>=6 km/s) are observed towards the edges between 1.5–3.0 and 7.0–8.5 km, and between ~0.4-0.8 km in depth (marked by black arrows). For QC, after each FWI run, results were verified based on the data fitting between the observed data and the predicted data. Figure 8 shows a shot gather comparison for the final FWI velocity model shown in Figure 7c. A good fit was obtained between the observed data and the synthetics, establishing the correctness of the FWI velocity model. A qualitative comparison was also made based on the FWI velocity values and from the direct measurement in the boreholes (Fig 2a). A similar velocity range of ~5.7 – 6.3 km/s was obtained from the FWI inversion. FWI velocity model was also verified later based on the Common Image Gathers (CIGs) produced from the KPreSDM (Fig. 11).

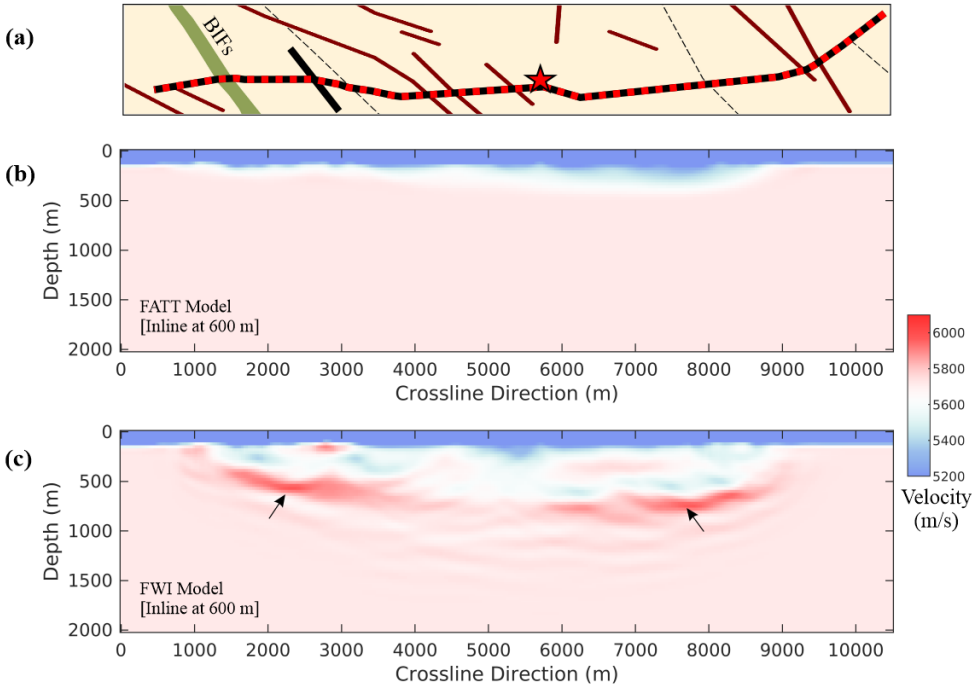

Figure 7. Comparison of velocity models. (a) Stripe of the geological map restricted to the computation domain (see Fig. 1), (b) FATT velocity model, and (c) FWI velocity model. Black arrows mark the accumulation of layered high velocities.

4.2 Depth Imaging

Ray-based KPreSDM & LS-KPreSDM, and wave-equation-based RTM were applied to obtain subsurface depth images. Both FATT and FWI velocity models were used for seismic imaging. Migrations were performed at a uniform grid spacing of 15 m on the same computational extent as was used for FATT and FWI. Both the velocity models were linearly extrapolated to match the migration grid. A Laplace filter was applied as the post-processing step to remove the low-frequency noise and to enhance the structural details. All migrations were performed using the 'Reveal' software (courtesy: Shearwater Geoservices).

https://doi.org/10.5194/egusphere-2026-3292
Preprint. Discussion started: 26 June 2026

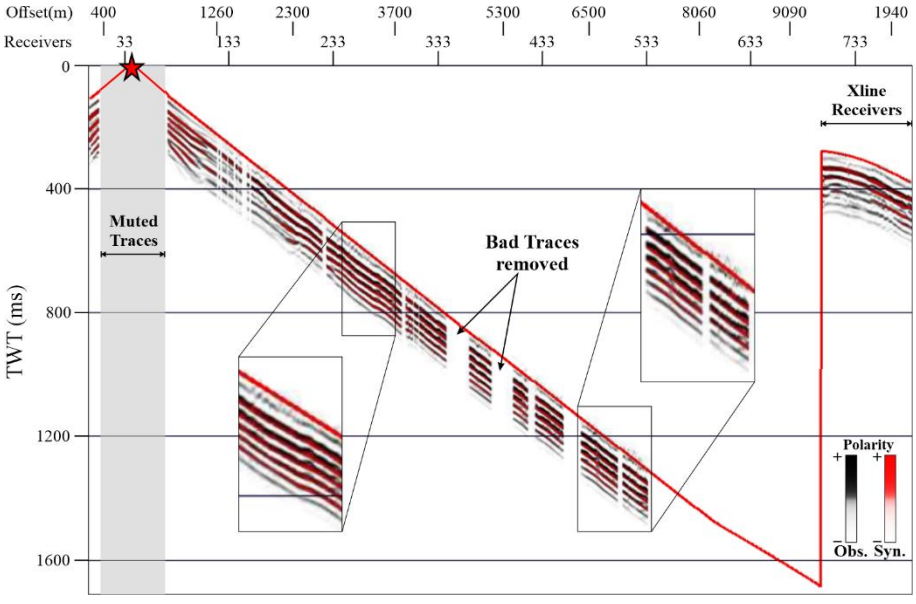

Figure 8. Shot gather comparison of observed data (black & white amp.) with superimposed synthetic data produced using FWI velocity model shown in Figure 7c (red & white amp.).

4.2.1 (Least-squares) Kirchhoff Prestack Depth Migration

The migration aperture for KPreSDM was set to 0–70° angle from the vertical and 3 km in distance. A 10% aperture and angle taper were applied to suppress migration noise at the edges. An equal aperture ratio was used in all directions. Migration was performed at every 10th inline position and at all crossline positions. KPreSDM was performed using both FATT (Fig. 9b) and FWI velocity models. In the latter case, a comparable imaging quality was obtained. In principle, we should expect a better depth image with a higher resolution velocity model, but such a situation was not observed here. It may be partially due to the relatively limited velocity details with depth of the FWI model (~0.5-1 km), and FATT, compared to the depth of interest (>1-2 km), i.e., the magma conduit (see Fig. 3). It might also be due to the limitation of the ray-based KPreSDM algorithm, which limits its ability to handle mainly the primary reflections against the geologically complex KDI where one can expect all kinds of arrivals (primaries, diffractions, diffracted reflections, etc.). Therefore, we tested LS-KPreSDM using the FATT velocity model to obtain the depth image with better amplitude fidelity (Fig. 9c). The same migration parameters were applied for the LS-KPreSDM as were used for the KPreSDM. 15 iterations of least-squares conjugate-gradient was performed until an improvement in terms of overall imaging was observed. Compared to KPreSDM, LS-KPreSDM produced lower-resolution but significantly more focussed results (compare Fig. 9c with 9b). Red arrows mark the areas with clear improvements. A slightly less focused image towards the NE edge was obtained where the velocity model was least constrained due to the crookedness of the profile (black arrow, Fig. 9c). This establishes the merit of applying the LS-KPreSDM method to obtain high-fidelity amplitude images in the hardrock environment.

https://doi.org/10.5194/egusphere-2026-3292
Preprint. Discussion started: 26 June 2026

4.2.2 Reverse Time Migration (RTM)

RTM is a two-way wave-equation-based seismic imaging method with the ability to better handle complex geological settings, such as the KDI. A 70 Hz minimum-phase Ricker wavelet was used as the source wavelet with a convolutional perfectly matched layer boundary condition. An offset-dependent aperture was defined with 10% taper at the edges. A 1 x 3 km aperture in the inline and crossline direction was used. A zero-lag cross-correlation was used as the imaging condition. Migration was performed at the optimum grid spacing and timestep to minimise the spatial/numerical dispersion. All migrated shot gathers were stacked to produce the final stacked section. Like KPreSDM, RTM imaging was also performed using both FATT and FWI velocity models (Fig. 10). Compared to ray-based KPreSDM, RTM with the FATT velocity model produced cleaner and more focused depth images (compare Fig. 10b with 9b). RTM with FWI velocity model further improved the mapped reflectivity (red arrows, compare Fig. 10c with 10b). Like LS-KPreSDM, less focus was achieved on the south-western end of the profile. A cluster of reflections was observed on the north-eastern edge (black arrows, Fig. 10c), compare with Fig. 10b and 9c). To further validate the fidelity of the FWI velocity model, offset-domain Common Image Gathers (CIGs) were produced using KPreSDM, given the high computational cost for RTM. CIGs were examined at various inline/crossline positions. Figure 11 shows the offset-domain CIG for several crossline positions along the inline direction (see Fig. 9b for reference). Flatness of the reflections at various depths validates the correctness of the FWI velocity model (red arrows).

5. Interpretation and Discussion

Advanced seismic imaging produced detailed depth images, and has tremendously enhanced the structural interpretation of the KDI. The interpretation was guided by multiple complementary datasets, including the CEM, Koillismaa borehole data, joint CSEM-MT results, magnetic and gravity data, and the existing geological framework of the area. Among the tested approaches, RTM using an FWI derived velocity model (RTM-FWI) produced the most focused and least noisy depth image; therefore, the following discussion is primarily based on this result.

5.1 Comparison of RTM-FWI Results with the Common Earth Model

Figure 12 shows the RTM-FWI result with the available CEM (see section 2.3 for details). Figure 12a shows the interpreted RTM-FWI result, and Figure 12b shows the CEM, borehole, and the BIFs overlaid on the seismic image. Solid brown outlay in Figure 12a is the traced outer boundary of the mafic intrusion, i.e., KDI (Fig. 12b). Solid black lines represent the up-dip facing slanted reflectors likely representing the mafic dykes/faults known in the area. Dashed-black lines mark the near-horizontal reflectivity. This might be suggestive of the overlying granites on top of the mafic intrusion. The red-dashed line on the south-western end of the profile likely represents a regional fault whose surface exposure extends beyond the known BIFs. The exact origin of this regional-scale reflector is not known, but it might represent the southern end of the (half-) graben formed during the rifting in an extensional setting associated with the genesis of the KLIC. The reflector marked by the blue line likely represents the extension of the south-eastern dipping reverse thrust fault cross-cutting the mafic intrusion (grey

https://doi.org/10.5194/egusphere-2026-3292
Preprint. Discussion started: 26 June 2026

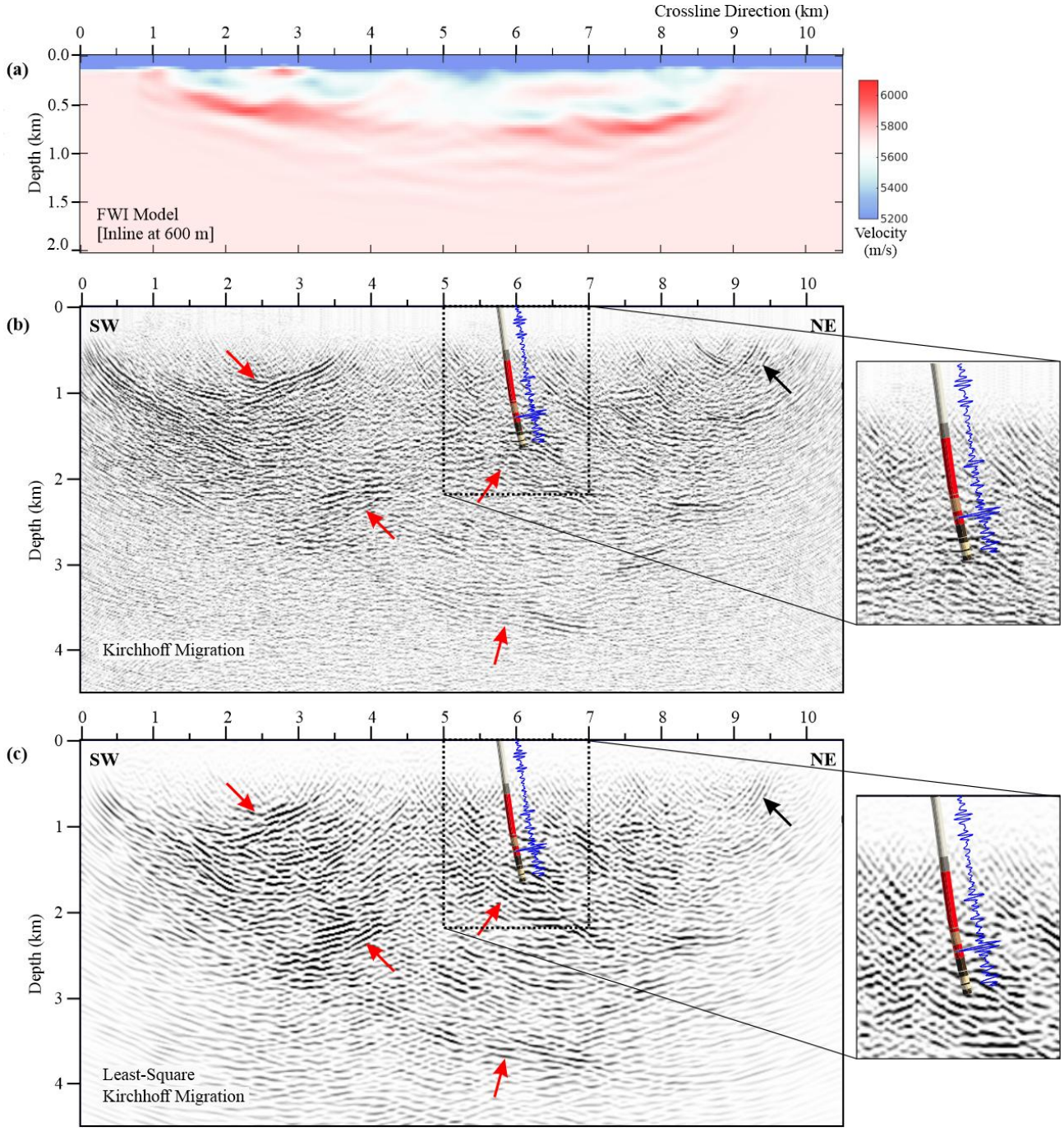

Figure 9. Comparison of KPreSDM results. (a) Stripe of the geological map restricted to the computation domain (see Fig.1), (b) KPreSDM, and (c) LS-KPreSDM for the FATT velocity model. Red arrows mark areas with better focusing, and black arrows mark the areas with diminished reflectivity. The blue curve shows the synthetic seismogram calculated using the petrophysical data (same as in Fig. 2e).

https://doi.org/10.5194/egusphere-2026-3292
Preprint. Discussion started: 26 June 2026

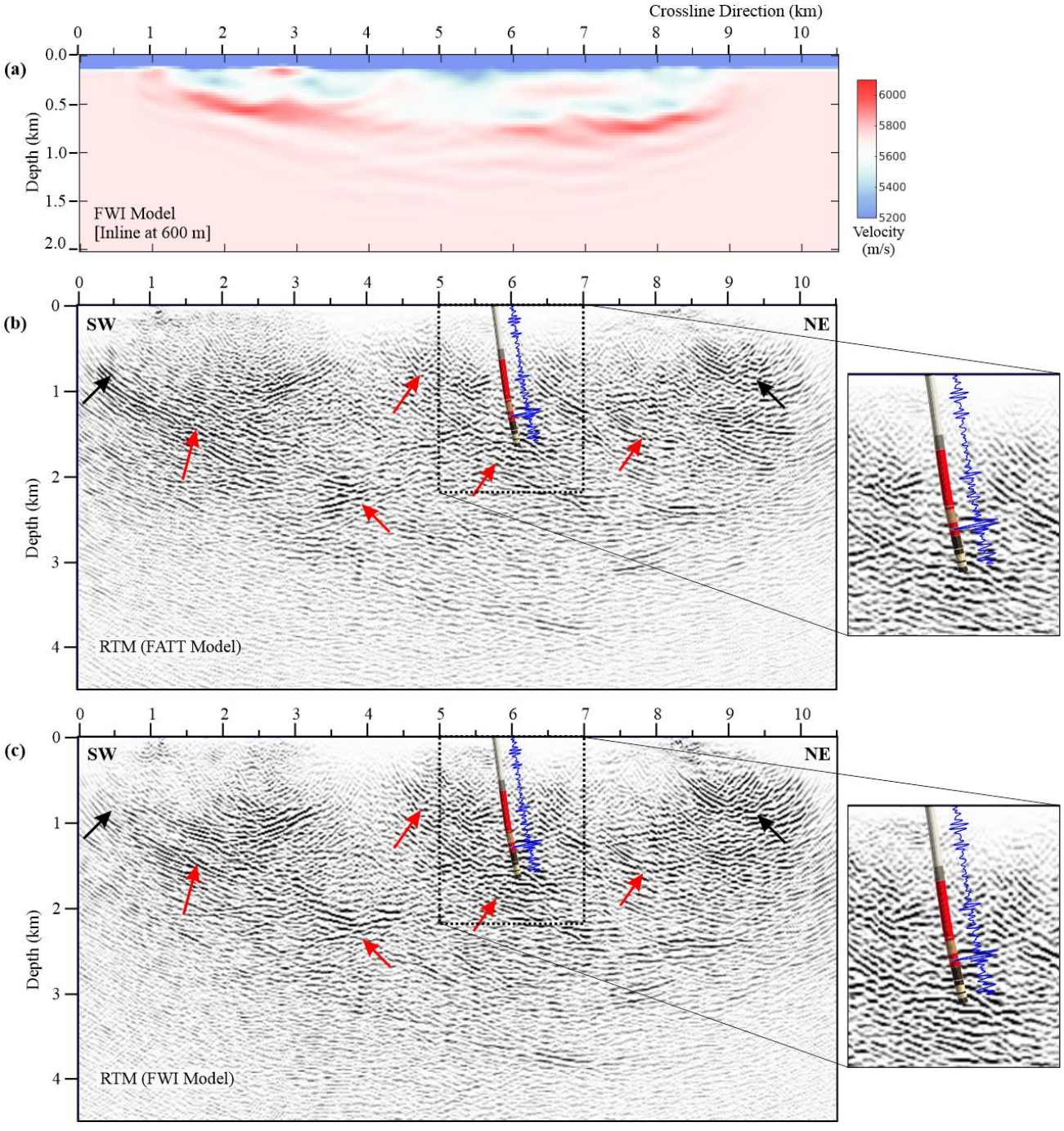

Figure 10. RTM results for (a) FATT, and (b) FWI velocity models. Red arrows mark areas of improvement. The top panel shows the FWI velocity model (same as in Fig. 7b). The blue curve shows the synthetic seismogram calculated using the petrophysical data (same as in Fig. 2e).

https://doi.org/10.5194/egusphere-2026-3292
Preprint. Discussion started: 26 June 2026

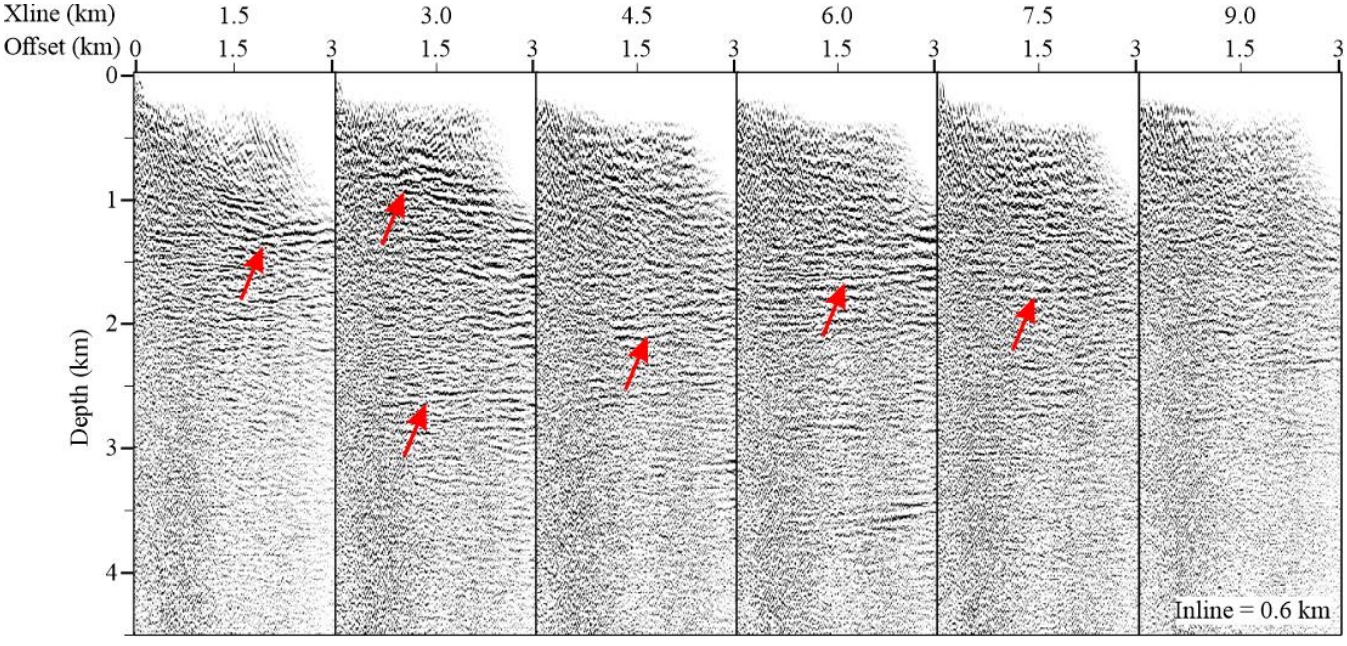

Figure 11. Common Image Gathers obtained from KPreSDM using FWI velocity model (inline position at 600 m). Red arrows mark the flatness of the reflectors.

surface, Fig. 3). The fault was interpreted to have uplifted the north-western part of the KDI and correlates with the known Oulujarvi shear zone (see Fig. 1, Lahtinen et al., 2023). The black arrow marks the reflectivity associated with lithological variations within the mafic intrusion confirmed by the borehole data (see Fig. 2f). The dashed-brown line marks the newly interpreted extension of the mafic intrusion based on the updated imaged seismic reflectivity in the area. It suggests the horizontal lateral extension of the mafic intrusion towards the north-east. This interpretation is mainly driven by the high acoustic impedance contrast between the magma conduit and the overlying granites (see Fig. 2c). A very small impedance response is expected from the granites and the Archean gneissic basement due to their similar velocity and density properties as per the petrophysical evidence. Additionally, there are known events of large-scale shear fracturing in the area, due to which the impedance properties of different lithologies may vary significantly. Therefore, in the absence of direct information, i.e., from boreholes or other independent confirmations, it is difficult to determine whether the laterally extending reflectivity is of mafic origin or has resulted from the granite-gneissic basement contact in the presence of abundant faults/dykes in the area. To minimize the uncertainty, seismic results were compared with the available CSEM-MT, gravity and aeromagnetic results.

5.2 Comparison of RTM-FWI results with joint CSEM-MT, gravity and aeromagnetics

Figure 13 shows the RTM-FWI result compared with the joint CSEM-MT results obtained under the SEEMS DEEP project (Vedrine et al., 2024). Only a qualitative interpretation has been attempted, as both methods measure different physical properties of the subsurface; a direct and unique correlation of the resistivity with the lithologies is not possible. Nevertheless,

https://doi.org/10.5194/egusphere-2026-3292
Preprint. Discussion started: 26 June 2026

lithologies can still be broadly distinguished based on the overall resistivity response. Figure 13b shows a good correlation between the seismic and CSEM-MT results. A thick package of high resistivity (between ~0.5–3 km in depth, marked by the black arrow) suggests the presence of a single or compositionally similar lithology. This package is in good agreement with the marked extension of the mafic intrusion (dashed brown line in Fig. 12a), supporting the hypothesis that the mafic–ultramafic rocks might be extending further towards the north-east than defined by the current CEM.

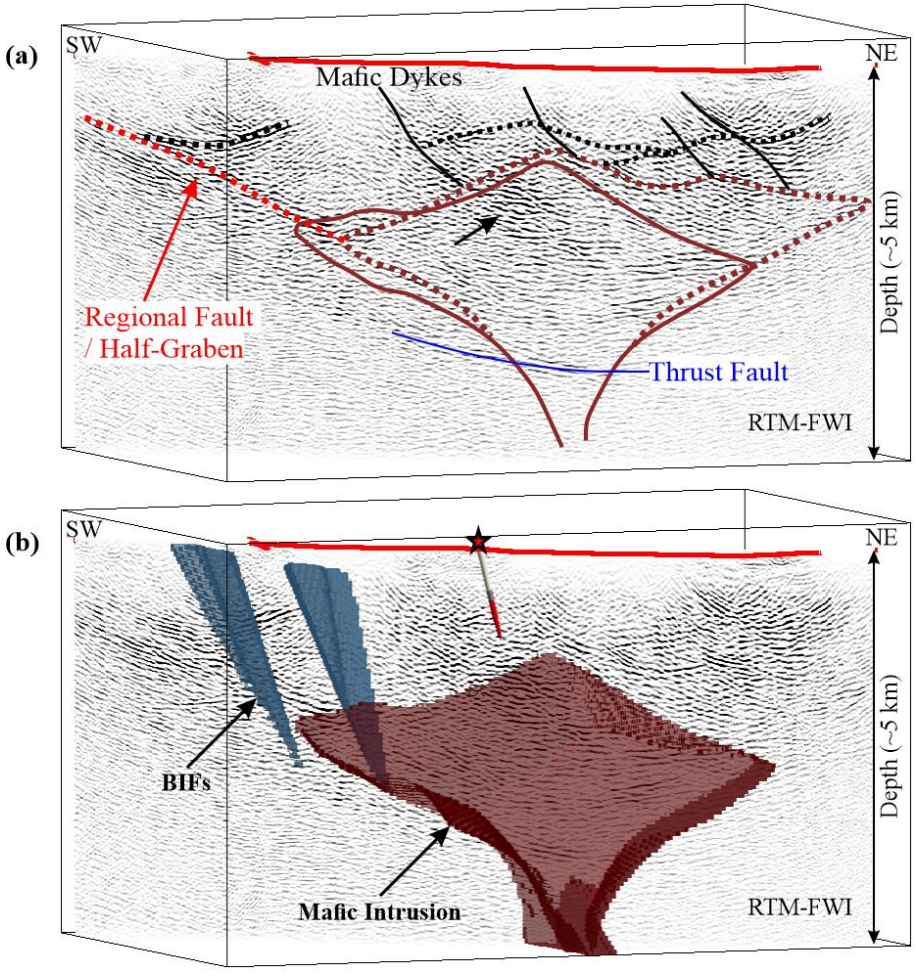

Figure 12. (a) Interpreted RTM-FWI result, and (b) is the same as (a) with CEM (brown surface), Koillismaa borehole (red star) and banded iron formation (BIFs) in the area. Dashed black lines in (a) show near-horizontal reflectivity, while solid black lines show up-dip reflectors. Solid brown line in (a) outlines the outer traced boundary of the CEM in (b), whereas the dashed brown line shows the updated extension of the CEM based on the RTM-FWI results. Solid red line marks the receiver positions.

To further confirm the proposed hypothesis, RTM-FWI results were compared with the aeromagnetic data (Fig. 14). The shallow reflectors (less than ~1 km, marked by black arrows) correlated well with the unexposed mafic dykes observed in the

https://doi.org/10.5194/egusphere-2026-3292
Preprint. Discussion started: 26 June 2026

aeromagnetic survey. Interestingly, shallow seismic reflectivity is also missing for the area where such feeder dykes are not observed (seismically transparent zone), providing strong evidence of their mafic origin. Figure 15 shows the comparison of RTM-FWI results with the gravity data. Combined with the seismic, CSEM and aeromagnetic data, it is apparent that the shifted magnetic high with respect to the gravity high is due to the near-surface mafic dykes (see Fig. 1 for comparison). A shift in the gravity high towards the north is most likely driven by the dense mafic intrusion against the overlying granites or the Archean gneissic basement, both having equivalent densities (see Fig 2b). Therefore, the interpreted horizontal lateral extension of the mafic intrusion towards the north (dashed brown line in Fig. 12a) is the most favourable scenario. This being considered exact, this also implies that the other half of the graben structure forming the KDI (see Fig. 12a) should be present further northwards and is beyond the reach of the current seismic profile. Otherwise, without the northwardly extending mafic intrusion, the only other possibility of a shifted gravity high is attributed to the root of the mafic intrusion (CEM, Fig. 12). It is possible that the root of the mafic intrusion is not strictly vertical but rather approaches the surface at a slant angle. A likely movement of the magma based on the observed seismic reflectivity is shown by the black arrow in Figure 15. This might have then shifted the net vertical density distribution of the KDI towards the north, and hence a northward-shifted gravity high was observed.

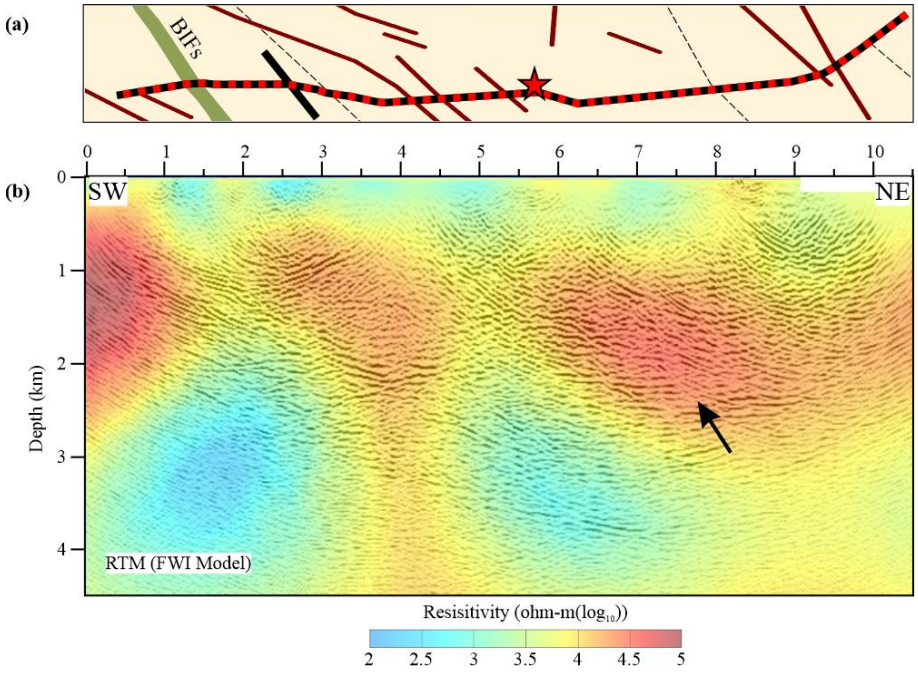

Figure 13. Comparison of RTM–FWI with CSEM-MT result. (a) Stripe of the geological map restricted to the computational domain (see Fig. 1) (b) Joint CSEM-MT result overlaid on the RTM-FWI image. The black arrow marks a package of high resistivity lithology.

https://doi.org/10.5194/egusphere-2026-3292
Preprint. Discussion started: 26 June 2026

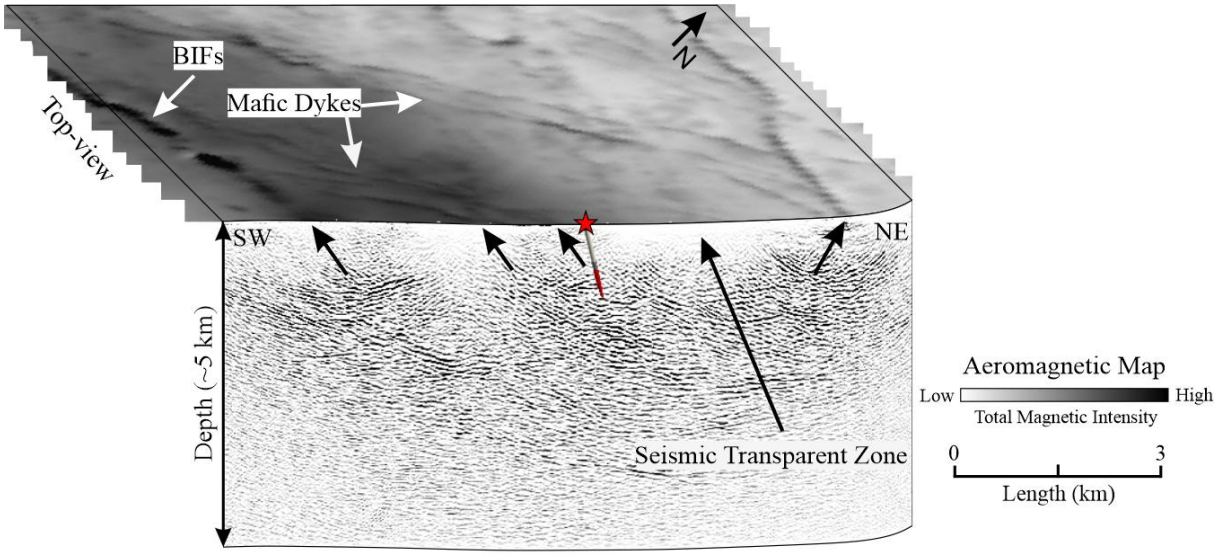

Figure 14. RTM-FWI result compared to aeromagnetics (Total Magnetic Intensity). Black arrows mark the correlation of the imaged near-surface reflectors with the unexposed mafic dykes. Red star marks the Koillismaa borehole.

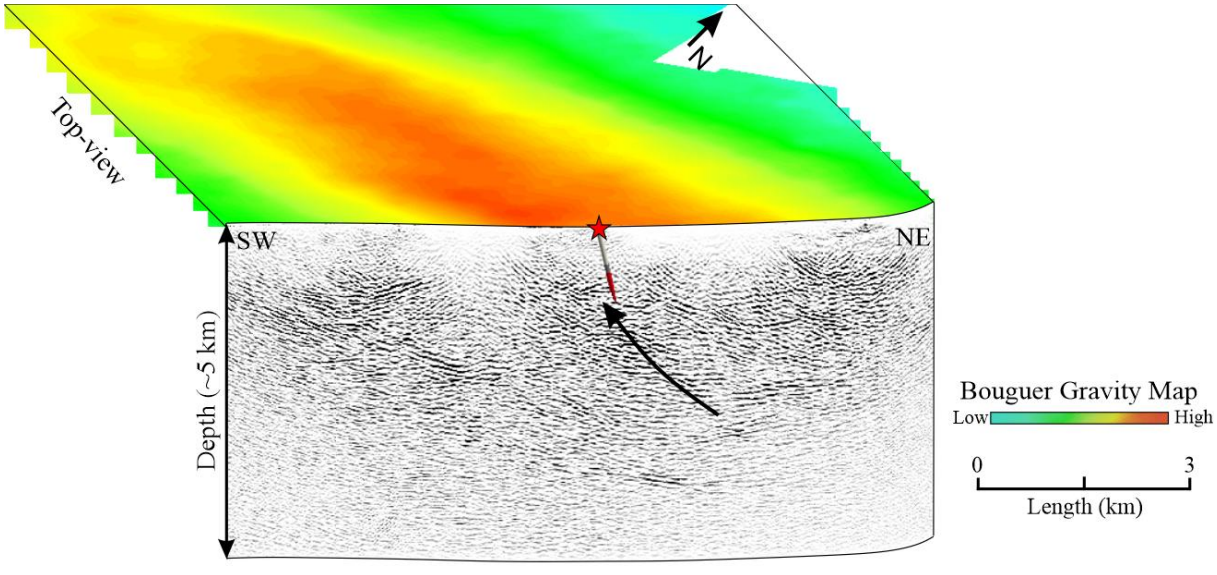

Figure 15. RTM-FWI result compared to the Bouguer gravity. The black arrow marks the interpreted movement of the magma towards the surface. Red star marks the Koillismaa borehole.

6. Conclusion

A regional reflection seismic profile was acquired to better understand the geometrical architecture of the KDI in northern Finland. Advanced seismic imaging was performed to image the geologically complex KDI using KPreSDM, LS-KPreSDM and RTM using FATT, and FWI derived velocity models. Ray-based LS-KPreSDM, which has rarely been applied in the

https://doi.org/10.5194/egusphere-2026-3292
Preprint. Discussion started: 26 June 2026

hardrock setting, proved highly beneficial by producing focussed images compared to conventional KPreSDM. The wave-equation-based joint RTM-FWI workflow produced the most optimal images of the KDI. A multi-method integrated approach was followed for the geophysical interpretation of the seismic imaging results using the existing CEM and borehole data, joint CSEM-MT results, and potential field method results. A comprehensive regional reinterpretation of the study area was done, and a better geometrical definition of the KDI was established. Shallow seismic reflectivity showed good correlation with the mafic dykes observed in the aeromagnetic data, whose origins were previously unknown. New advanced seismic imaging delineated a more laterally extending top of the KDI towards the north, which was not recognized previously. It is interpreted that the dense mafic intrusion associated with this lateral extension might have shifted the net vertical mass distribution of the subsurface, and hence have attributed to the spatial offset shift in the gravity high and magnetic high in the KLIC area. A separate hypothesis regarding this observed shift has been proposed discussing the possibility of an oblique approach of the magma towards the surface, rather than a pure vertical emplacement. Before this study, the magma emplacement was believed to be purely vertical.

Data availability

Data associated with this research are available per request to the project coordinator: Uula Autio (uula.autio@gtk.fi), Geological Survey of Finland, Vuorimiehentie 5, 02151 Espoo, Finland.

Author contribution

AG and MM obtained the funding. BS, AG and MM contributed to the survey design and data acquisition. BS and AG contributed to the velocity model building (FATT and FWI; data preprocessing, inversion and result verification). AG introduced the necessary modifications in the FWI source code. BS performed the signal processing and migration for KPreSDM, LS-KPreSDM and RTM. BS and TK interpreted the results. BS wrote the manuscript's main content with contributions from TK, AG and MM. All authors contributed to the final discussion of the results.

Competing interests

Editorship CI! The authors have the following competing interests: At least one of the (co-)authors is a member of the editorial board of Natural Hazards and Earth System Sciences.

https://doi.org/10.5194/egusphere-2026-3292
Preprint. Discussion started: 26 June 2026

Acknowledgments

We are greatly thankful to the entire SEEMS DEEP group for successfully concluding the project. Globe Claritas™ under the academic license from Petrosys Ltd., and Seismic Unix were used for the data processing and visualization. We thank Romain Brossier (ISTerre) and Ludovic Metivier (ISTerre/LJK) for providing us with the TOYXDAC_TIME, 3D viscoacoustic FWI code developed in the framework of the SEISCOPE Consortium (https://seiscope2.osug.fr, last access: September 2024). GeoTomo Inc. TomoPlus software was used for the travel-time tomography. We thank Yousef Amirzadeh for his extended help in the first arrival picking of the data. We thank Shearwater Geoservices for granting us an academic licence of Reveal software to run KPreSDM, LS-KPreSDM and RTM. Thanks to Mira Geoscience for special licensing terms to use the Geoscience Analyst Pro software for interpretation. We thank the Polish high-performance computing infrastructure PLGrid (HPC Centre: ACK Cyfronet AGH) for providing the HPC facilities and support within the computational grant no. PLG/2024/017350.

Financial support

SEEMS DEEP was part of the ERA-MIN3 Joint call 2021 (National funding agencies: Finland: Business Finland (640/31/2022), France: ANR (ANR-22-MIN3-0006-02), Sweden: VINNOVA (2022-00209), Poland: NCBR (ERA-MIN3/1/113/SEEMSDEEP/2022).

References

Alapieti, T., Lahtinen, J.: Platinum-group element mineralization in layered intrusions of northern Finland and the Kola Peninsula, Russia, in: The geology, geochemistry, mineralogy and mineral beneficiation of platinum-group elements, Canadian Institute of Mining, Metallurgy and Petroleum, vol. CIM Special Volume, 507–546, 2002.

Adamczyk, A., Malinowski, M., and Górszczyk, A.: Full-waveform inversion of conventional Vibroseis data recorded along a regional profile from southeast Poland, Geophys. J. Int., 203, 351–365, https://doi.org/10.1093/gji/ggv305, 2015.

Afanasiev, M. V., Pratt, R. G., Kamei, R., and McDowell, G.: Waveform-based simulated annealing of crosshole transmission data: a semi-global method for estimating seismic anisotropy, Geophys. J. Int., 199, 1586–1607, https://doi.org/10.1093/gji/ggu307, 2014.

Autio, U., Darnet, M., Górszczyk, A., Kamm, J., Heinonen, S., Malinowski, M., Kim, B., Singh, B., Vedrine, S., Bretaudeau, F., Patzer, C., Karinen, T., Kalscheuer, T., Truffert, C., Wojdyła, M., Kivinen, A., and Koltun, Y.: Integrating Seismic and Electromagnetic Methods for Deep Mineral Exploration – Results from the SEEMS DEEP Project, NSG 2024 5th Conference on Geophysics for Mineral Exploration and Mining, 1–5, https://doi.org/10.3997/2214-4609.202420147, 2024.

Baeten, G., Maag, J. W. de, Plessix, R.-E., Klaassen, R., Qureshi, T., Kleemeyer, M., ten, Kroode, F., and Rujie, Z.: The use of low frequencies in a full-waveform inversion and impedance inversion land seismic case study, Geophys. Prospec., 61, 701–711, https://doi.org/10.1111/1365-2478.12010, 2013.

https://doi.org/10.5194/egusphere-2026-3292
Preprint. Discussion started: 26 June 2026

Bräunig, L., Buske, S., Malehmir, A., Bäckström, E., Schön, M., and Marsden, P.: Seismic depth imaging of iron-oxide deposits and their host rocks in the Ludvika mining area of central Sweden, Geophysical Prospecting, 68, 24–43, https://doi.org/10.1111/1365-2478.12836, 2020.

Burschil, T., Köhn, D., Körbe, M., Gabriel, G., Großmann, J., Firla, G., and Fiebig, M.: Seismic data acquisition to combine high-resolution seismic reflection and full-waveform inversion – a case study for overdeepened valleys, Solid Earth, 16, 1493–1507, https://doi.org/10.5194/se-16-1493-2025, 2025.

Ding, Y. and Malehmir, A.: Reverse time migration (RTM) imaging of iron oxide deposits in the Ludvika mining area, Sweden, Solid Earth, 12, 1707–1718, https://doi.org/10.5194/se-12-1707-2021, 2021.

Gislason, G., Heinonen, S., Salmirinne, H., Konnunaho, J., and Karinen, T.: KOSE - Koillismaa Seismic Exploration survey: Acquisition, processing and interpretation, 2019.

Górszczyk, A., Malinowski, M., and Bellefleur, G.: Enhancing 3D post-stack seismic data acquired in hardrock environment using 2D curvelet transform, Geophysical Prospecting, 63, 903–918, https://doi.org/10.1111/1365-2478.12234, 2015.

Hayward, N.: Improving Multiscale Structural Targeting Precision for Large Ni-Cu (±PGE, Co) Sulfide Discoveries from Global Case Studies, Economic Geology, 119(8), 1745–1767, doi: https://doi.org/10.5382/econgeo.5117, 2024.

Heinonen, S., Nousiainen, M., Karinen, T., and Häkkinen, T.: Are Seismic P-Wave Velocities Capable of Revealing The Deep-Seated Prospective Intrusion?, NSG2022 4th Conference on Geophysics for Mineral Exploration and Mining, 1–5, https://doi.org/10.3997/2214-4609.202220167, 2022.

Hloušek, F., Jusri, T., Buske, S., Heinonen, S., Karinen, T., Kozlovskaya, E., and Leväniemi, H.: Seismic imaging of the crustal structure in the Sodankylä region (Finland): unveiling the Central Lapland Greenstone Belt's mineral potential, Geophysical Journal International, 241, 338–353, https://doi.org/10.1093/gji/ggaf053, 2025.

Järvinen, V., Halkoaho, T., Konnunaho, J., Heinonen, J. S., and Rämö, O. T.: Parental magma, magmatic stratigraphy, and reef-type PGE enrichment of the 2.44-Ga mafic-ultramafic Näränkävaara layered intrusion, Northern Finland, Miner Deposita, 55, 1535–1560, https://doi.org/10.1007/s00126-019-00934-z, 2020.

Järvinen, V., Karampelas, N., Rämö, O. T., Halkoaho, T., Törmänen, T., Mikkola, P., and Lahaye, Y.: Secular change of tectonic setting in the Archean Takanen greenstone belt, northeastern Karelia Province, Fennoscandian Shield, Bulletin of the Geological Society of Finland, Vol. 95, https://doi.org/10.17741/bgsf/95.2.002, 2023.

Karinen, T.: The Koillismaa Intrusion, northeastern Finland - evidence for PGE reef forming processes in the layered series, 2010.

Karinen, T., Lahti, I., Konnunaho, J., and Salo, A.: The Koillismaa Deep Hole: insight to anomalous mafic intrusion, ARLIN – Online Workshop 1 (Apatity, 25.02.2021), 38–41, https://doi.org/10.31241/ARLIN.2021.009, 2021.

Karinen, T., Kurhila, M., Moilanen, M., Konnunaho, J., Salmirinne, H., and Tirroniemi, J.: Chilled margin and marginal reversal formation in the Koillismaa Deep Intrusion: implications for parental magma compositions in the 2.44 Ga Tornio–Näränkävaara Belt, Contrib Mineral Petrol, 180, 43, https://doi.org/10.1007/s00410-025-02226-4, 2025.

Köykkä, J., Lahtinen, R., and Manninen, T.: Tectonic evolution, volcanic features and geochemistry of the Paleoproterozoic Salla belt, northern Fennoscandia: From 2.52 to 2.40 Ga LIP stages to ca. 1.92–1.90 Ga collision, Precambrian Research, 371, 106597, https://doi.org/10.1016/j.precamres.2022.106597, 2022.

https://doi.org/10.5194/egusphere-2026-3292
Preprint. Discussion started: 26 June 2026

Lahtinen, R., Köykkä, J., Salminen, J., Sayab, M., and Johnston, S. T.: Paleoproterozoic tectonics of Fennoscandia and the birth of Baltica, Earth-Science Reviews, 246, 104586, https://doi.org/10.1016/j.earscirev.2023.104586, 2023.

Makkonen, V.: Korpuan Jatkotutkimus, Rautaruukki Oy, 1972.

Malinowski, M., Operto, S., and Ribodetti, A.: High-resolution seismic attenuation imaging from wide-aperture onshore data by visco-acoustic frequency-domain full-waveform inversion: Attenuation imaging, Geophys. J. Int., 186, 1179–1204, https://doi.org/10.1111/j.1365-246X.2011.05098.x, 2011.

Malinowski, M., Brodic, B., Martinkauppi, I., Koskela, E., and Laakso, V.: Distributed acoustic sensing vertical seismic profiling in hardrock environment: case study from Koillismaa drillhole, Finland, 84th EAGE Annual Conference & Exhibition, 1–5, https://doi.org/10.3997/2214-4609.2023101043, 2023.

Malinowski, M., Karinen, T., Autio, U., Heinonen, S., Singh, B., Górszczyk, A., Sito, Ł., and the SEEMS DEEP Working Group: Uncovering the deep structure of the Koillismaa Layered Intrusion Complex, Finland using a novel 3D seismic survey, Solid Earth, 16, 1437–1452, https://doi.org/10.5194/se-16-1437-2025, 2025.

Métivier, L. and Brossier, R.: The SEISCOPE optimization toolbox: A large-scale nonlinear optimization library based on reverse communication, Geophysics, 81, F1–F15, https://doi.org/10.1190/geo2015-0031.1, 2016.

Métivier, L., Allain, A., Brossier, R., Mérigot, Q., Oudet, E., and Virieux, J.: Optimal transport for mitigating cycle skipping in full-waveform inversion: A graph-space transform approach, Geophysics, 83, R515–R540, https://doi.org/10.1190/geo2017-0807.1, 2018.

Montana, F., Cellura, M., Di Silvestre, M.L., Longo, S., Luu, L.Q., Riva Sanseverino, E., Sciumè, G.: Assessing Critical Raw Materials and Their Supply Risk in Energy Technologies—A Literature Review. Energies, 18, 86, https://doi.org/10.3390/en18010086, 2025.

Norman, M., To, R. T. T., Chua, M. L., and Huang, M.: Oak Dam Sparse 3D Seismic Application: Geological Model and IOCG Exploration Implications, NSG 2024 5th Conference on Geophysics for Mineral Exploration and Mining, 1–5, https://doi.org/10.3997/2214-4609.202420180, 2024.

Nousiainen, M., Heinonen, S., and Karinen, T.: Petrophysics of the Koillismaa drill hole, LITHOSPHERE 2022: Twelfth symposium on structure, composition and evolution of the lithosphere, 131–134, https://doi.org/http://hdl.handle.net/10138/350596, 2022.

Pratt, R. G.: Seismic waveform inversion in the frequency domain; Part 1, Theory and verification in a physical scale model, Geophysics, 64, 888–901, https://doi.org/10.1190/1.1444597, 1999.

Ravaut, C., Operto, S., Improta, L., Virieux, J., Herrero, A., and Dell'Aversana, P.: Multiscale imaging of complex structures from multifold wide-aperture seismic data by frequency-domain full-waveform tomography: application to a thrust belt, Geophys. J. Int., 159, 1032–1056, https://doi.org/10.1111/j.1365-246X.2004.02442.x, 2004.

Salmirinne, H. and Iljina, M.: Koillismaan kerrosintruusiokompleksin tulokanavamuodostuman painovoimatulkinta ja alueen malmimahdollisuudet (osa 1) - Publications, reports, maps and posters, 2003.

Schijns, H., Townsend, J., Haddow, D., Shawcross, M., and Ehrig, K.: Sparse 3D seismic survey over the Olympic Dam IOCG deposit, 1658–1662, https://doi.org/10.1190/image2023-3908343.1, 2023.

https://doi.org/10.5194/egusphere-2026-3292
Preprint. Discussion started: 26 June 2026

Simandl, G. J., and Paradis, S.: Vanadium as a critical material: economic geology with emphasis on market and the main deposit types, Applied Earth Science, 131, 218–236, https://doi.org/10.1080/25726838.2022.2102883, 2022.

Singh, B., Malinowski, M., Hloušek, F., Koivisto, E., Heinonen, S., Hellwig, O., Buske, S., Chamarczuk, M., and Juurela, S.: Sparse 3D Seismic Imaging in the Kylylahti Mine Area, Eastern Finland: Comparison of Time Versus Depth Approach, Minerals, 9, https://doi.org/10.3390/min9050305, 2019.

Singh, B., Malinowski, M., Górszczyk, A., Malehmir, A., Buske, S., Sito, Ł., and Marsden, P.: 3D high-resolution seismic imaging of the iron oxide deposits in Ludvika (Sweden) using full-waveform inversion and reverse time migration, Solid Earth, 13, 1065–1085, https://doi.org/10.5194/se-13-1065-2022, 2022.

Singh, B., Górszczyk, A., Malinowski, M., Heinonen, S., Autio, U., Karinen, T., Wojdyła, M., and the SEEMS DEEP Working Group: 2D seismic imaging of the Koillismaa Layered Igneous Complex, north-eastern Finland, Solid Earth, 16, 1137–1151, https://doi.org/10.5194/se-16-1137-2025, 2025.

Skyttä, P., Piippo, S., Kloppenburg, A., and Corti, G.: 2. 45 Ga break-up of the Archaean continent in Northern Fennoscandia: Rifting dynamics and the role of inherited structures within the Archaean basement, Precambrian Research, 324, 303–323, https://doi.org/10.1016/j.precamres.2019.02.004, 2019.

Stopin, A., Plessix, R.-É., and Al Abri, S.: Multiparameter waveform inversion of a large wide-azimuth low-frequency land data set in Oman, Geophysics, 79, 69–77, https://doi.org/10.1190/geo2013-0323.1, 2014.

Tarantola, A.: A strategy for nonlinear elastic inversion of seismic reflection data, Geophysics, 51, 1893–1903, https://doi.org/10.1190/1.1442046, 1986.

Tirroniemi, J., Bischoff, A., Malinowski, M., Uula, A., Karinen, T., Lukkarinen, V., Heinonen, S., Mikkola, P., Leskelä, T., Patzer, C., Piipponen, K., Nousiainen, M., Hakala, P., Martinkauppi, I., Anttilainen, T., Engström, J., Konnunaho, J., Telkkälä, P., and Haavikko, S.: Koillismaa Deep Hole Final Report, 2024.

Védrine, S., Patzer, C., Bretaudeau, F., Rochlitz, R., Autio, U., Kim, B., Vermeersch, F., Kamm, J., Truffert, C., and Darnet, M.: Joint inversion of MT and CSEM data for Deep Mineral Exploration: Case Study of Koillismaa Layered Intrusion Complex, 26th EM Induction Workshop, 1–4, 2024.

Virieux, J. and Operto, S.: An overview of full-waveform inversion in exploration geophysics, Geophysics, 74, WCC1–WCC26, https://doi.org/10.1190/1.3238367, 2009.

Zhang, J. and Toksoz, M. N.: Nonlinear refraction traveltime tomography, Geophysics, 63, 1726–1737, https://doi.org/10.1190/1.1444468, 1998.

Ziramov, S., Young, C., Kinkela, J., Turner, G., and Urosevic, M.: Pre-stack depth imaging techniques for the delineation of the Carosue Dam gold deposit, Western Australia, Geophysical Prospecting, 71, 1077–1095, https://doi.org/10.1111/1365-2478.13314, 2023.